Title: Dissecting compounded hepatocyte injury in a model of MASLD progression from human induced pluripotent stem cells

Authors: Julian Weihs*[1], Fatima Baldo*[2], Alessandra Cardinali*[2,3], Gehad Youssef*[2], Katarzyna Ludwik[4], Harald Stachelscheid[4], Nils Haep[5,6], Peter Tang[5], Igor Sauer[5], Pavitra Kumar[7], Cornelius Engelmann[7,8], Susanna Quach[1], Philip Bufler[1], Namshik Han[2#], Milad Rezvani[1,6,9,10#]

Affiliations:

1. Charité Universitätsmedizin Berlin, Department of Pediatrics, Division of Gastroenterology, Nephrology and Metabolic Medicine, Augustenburger Platz 1, 13353 Berlin
2. Milner Therapeutics Institute, University of Cambridge
3. LifeArc, Lynton House, 7-12 Tavistock Square, London, WC1H 9LT
4. Berlin Institute of Health (BIH) at Charité – Universitätsmedizin Berlin, BIH Core Unit pluripotent Stem Cells and Organoids (CUSCO), Berlin, Germany
5. Department of Surgery, Campus Virchow-Klinikum, Experimental Surgery, Charité – Universitätsmedizin Berlin, Augustenburger Platz 1, 13353 Berlin, Germany
6. Clinician Scientist Program, Berlin Institute of Health at Charité (BIH), Anna-Louisa-Karsch-Str. 2, 10178 Berlin, Germany
7. Department of Hepatology and Gastroenterology, Medizinische Klinik m. S. Hepatologie und Gastroenterologie, Charité, Universitätsmedizin Berlin, Campus Virchow-Klinikum (CVK) and Campus Charité Mitte (CCM)
8. Berlin Institute of Health (BIH), 10178 Berlin, Germany
9. Berlin Institute of Health (BIH) at Charité-Universitätsmedizin Berlin, BIH Center for Regenerative Therapies (BCRT), Berlin, Germany
10. Division of Gastroenterology, Hepatology and Nutrition, Cincinnati Children's Hospital Medical Center, Cincinnati, OH 45229, USA

* Equally contributed to this work, # Corresponding Authors

Abstract:

Metabolic dysfunction-associated steatotic liver disease (MASLD) is a complex, multifactorial condition influenced by genetic predisposition, inter-organ signaling, and immune cell infiltration. The difficulty of modeling the complex nature of the disease makes it increasingly challenging to identify treatments that intercept its progression. Here, we show the suitability of cumulative injury modeling toward steatohepatitis from hepatocyte-like cells (HLCs) generated from human induced pluripotent stem cells (iPSCs). These include insults such as free fatty acid excess, soluble extra-hepatic signaling, pro-inflammatory immune cell co-culture and genomic modifiers (PNPLA3-I148M variant). We harness this model to elucidate the molecular and functional consequences of hepatocellular injury progression and identify suitable points of therapeutic interception. Both healthy and PNPLA3-I148M iPSC-donor derived HLCs developed high-level generic steatosis response, yet the PNPLA3-I148M line was more susceptible to mitochondrial injury by the adipokine resistin and the myokine myostatin. Co-culture with peripheral blood mononuclear cells (PBMCs) compounded the previous multi-hit injury. Further, transcriptomic data revealed inflammatory HLC reprogramming and loss of genomically encoded mitochondrial metabolism along injury progression. We demonstrate a nuanced spectral metabolic injury model, mirroring clinical MASLD progression, suitable for testing stage and donor-specific disease interceptions.

Abbreviations:

MASLD = Metabolic dysfunction-associated steatotic liver disease

MASH = Metabolic dysfunction-associated steatohepatitis

Res = Resistin

Myo = Myostatin

iPSCs = Induced pluripotent stem cells

HLCs = Hepatocyte-like cells

Wt = Wildtype

PBMCs = Peripheral blood mono-nuclear cells

OA = Oleic acid

PA = Palmitic acid

FCS = Fetal Calf Serum

LPS = Lipopolysaccharide

Introduction:

Metabolic dysfunction-associated steatotic liver disease (MASLD) is a multifactorial disease that poses a significant global public health concern, affecting approximately 30% of the worldwide population (Younossi et al., 2023). The multi-hit pathogenesis of the disease is generally well understood (Buzzetti et al., 2016). Substrate excess, genetic mutations and whole organ insulin resistance signaling cause the liver to respond with steatosis. Additionally, lipotoxicity causes subcellular stress in hepatocytes. Hepatic immune cell infiltration (as in Metabolic dysfunction-associated steatohepatitis or MASH), ultimately leads to fibrogenesis and potentially results in cirrhosis over time.

Regarding the multiple injuries in MASLD, steatosis and hepatocellular lipid toxicity are effects promptly seen clinically, as evidenced by for example by sonographic steatosis (Ferraioli & Monteiro, 2019). As MASLD is part of the organism-wide dysfunctions, secreted signaling molecules from adipose or muscle tissue, have been described in systemic inflammation and MASLD, albeit their functional impact on liver pathobiology remains elusive (Li & Wang, 2020). For example, the adipokine resistin (Res) has been associated with inflammation and liver disease (Ajmera et al., 2017). Myostatin (Myo), a myokine involved in sarcopenia, a co-morbidity often associated with MASLD, can e.g. activate hepatic stellate cells (Delogu et al., 2019) and is elevated in patients with liver disease (García et al., 2010). Further, murine myostatin knock-out protects from MASLD development (Wilkes et al., 2009). However, the functional impact of these factors and others on human hepatocytes is not well-resolved.

Pre-clinical models have been proposed for functional interrogation to dissect the multiple layers of injury. Numerous studies have demonstrated that human induced pluripotent stem cells (iPSCs) can model MASLD after hepatic differentiation (Rezvani et al., 2023). The generated hepatocyte-like cells (HLCs) can be harnessed to model subcellular lipotoxicity and the effect of the most common risk mutations, like the I148M variant of the gene PNPLA3 (Tilson et al., 2021). Although the addition of insulin has been shown (Kimura et al., 2022), the nuanced impact of non-visceral organs, especially muscle and adipose tissue, on MASLD progression has not been incorporated into current models. Furthermore, a roadmap for the multiple hits and potential compounded effects has yet to be defined. Such analysis would help to identify possible points for therapeutic intervention that is currently lacking.

Here, we dissect the compounded effects of multiple overlapping metabolic injuries on hepatocytes in an iPSC-derived model. We map out the response to steatosis and lipotoxicity alone and after incorporating muscle and adipose signals by resistin and myostatin, as well as inflammation–all against

the backdrop of genomic risk variation. Thus, we generate a spectral MASLD-to-MASH model suitable for testing stage-specific therapeutic interceptions.

Methods:

Cell lines

We used the two human iPSC donor lines BIHi001-B major homozygous for PNPLA3 rs738409 variant (PNPLA3-WT or I148I) and BIHi005-A minor homozygous for the PNPLA3 rs738409 variant (PNPLA3-I148M), provided by the BIH Core Unit Pluripotent Stem Cells and Organoids. Both cell lines are registered in the Human Pluripotent Stem Cell Registry (RRID:CVCL_YN70 and RRID:CVCL_IT56). We kept cells on vitronectin-coated (Thermo) plates in mTeSR medium (Stem Cell Tech). All experiments performed were done at 37°C in a 5% O_2 and 5% CO_2 hypoxic atmosphere.

Primary cells

Blood isolation was done in accordance with ethical standards of the Charité Universitätsmedizin Berlin and the amended Declaration of Helsinki. We obtained peripheral blood from one healthy individual to isolate mononuclear cells using Ficoll-Paque (Sigma). Precisely, we mixed whole blood with PBS (w/o Ca^{2+} Mg^{2+}) in a 1:1 ratio and overlaid this dilution on the Ficoll in a 3 to 2 ratio, respectively. We then centrifuged the mixture for 30 minutes at 300 g at room temperature, using the lowest levels of brake and acceleration. The leukocyte layer was transferred to a new tube and washed once with PBS. After lysing red blood cells by incubating the cells for 10 min in ACK lysis buffer, we washed twice, counted and froze cells down in a 10% DMSO solution in FCS using Mr. Frosty. The cells were stored in vapor phase liquid nitrogen below -135°C until further use.

Differentiation into hepatocyte-like cells (HLCs)

We adapted a 28-day published protocol to derive HLCs (Kajiwara et al., 2012).

First, we generated frozen stocks of ROCKi-adapted iPSCs by expanding cells under constant exposure to 10 µM ROCKi (Tocris) in mTeSR medium. From these cultures, we detached iPSCs using a 5 min incubation at room temperature with 0.5 mM EDTA in PBS, removal of the EDTA solution and resuspension in Bambanker freezing medium (NIPPON). These stocks we then froze using a Mr. Frosty container to -80°C and then transferred frozen stocks into vapor phase liquid nitrogen below -135°C. There cells remained until we initiated HLC differentiation.

Therefore, we thawed ROCKi-adapted iPSCs by incubating them in a water bath for 1 minute until a small ice crystal remained. The cryosolution was then transferred to a 15 ml Falcon tube, and 10 times the volume of room temperature mTeSR containing ROCKi was added dropwise to the solution. We centrifuged the cells for 3 min at 300 g and re-suspended them in ROCKi-containing mTeSR medium. After cells reached approximately 80% confluency in a 10 cm dish, we initiated HLC differentiation by single-cell splitting of ROCKi-adapted iPSCs on geltrex coated 6-well, 12-well or 24-well plates (Day 0). Then, we added definitive endoderm (DE)-Induction medium, consisting of RPMI1640, 2% B27 (Gibco), 1% PenStrep (Gibco), 100 ng/ml Activin A (Peprotech) and freshly added 50 ng/ml Wnt3 (RnD Systems), with 0.5 mM sodium butyrate (Sigma) for 5 days, and subsequently DE-Induction medium without sodium butyrate for one additional day. After DE induction, we added KO-medium containing KO-DMEM (Gibco), 20% KO Serum (Gibco), 1% PenStrep (Gibco), 1% Glutamax (Gibco), 1% Non-Essential Amino Acids (Lonza), 1% DMSO (PanBiotech) and 0.1 mM beta-mercaptoethanol for 7 days to induce hepatic commitment. Subsequently, we exposed cells for 7 days to HBM medium containing 20 ng/ml HGF (Peprotech), 20 ng/ml OSM (Miltenyi) and 1% PenStrep for hepatocyte commitment. We matured the cells for 7 days using complete HCM Bulletkit medium (Lonza, excluding EGF) either with or without the additional supplementation of 5 nM T3 (Tocris), 100 nM sodium selenite (NaSe; Sigma) and 100

µM CDCA (Sigma) according to recently published studies (Ma et al., 2022; Nell et al., 2022). On day 28, we either harvested cells or performed disease modeling.

Cumulative metabolic injury model

We tested different cumulative MASLD injury hit combinations in our HLC model. Generally, we exposed HLCs for 3 days to either free fatty acid excess alone (1 Hit), combined with the inter-organ signaling molecules resistin and myostatin (2 Hit) or in further addition with co-cultured peripheral blood mono-nuclear cells (PBMCs, 3 Hits).

We exposed cells to oleic and palmitic acid (OA and PA) in a 5 to 2 ratio on day 28 for 3 days to model free fatty acid excess. Oleic and palmitic acid (both Merck) were coupled to the HCM bulletkit derived BSA by incubation at 37°C for at least 2 h. Initial experiments (Fig. 1B and C) we performed using 700 µM total free fatty acid concentration. However, after titrating we adjusted the total concentration to 125 µM, since we saw a saturation of steatotic area from this concentration on (data not shown).

To account for inter-organ signaling in our model, we tested recombinant resistin and myostatin (both Peprotech), both using 100 ng/ml concentration. Factors were reconstituted according to manufacturer instructions. If included, we added these factors from day 28 on for three days.

For modeling inflammation, we included PBMCs in an indirect trans-well co-culture using Millicell trans-well inserts (Millipore) with a 0.4 µm pore size, 1 day after the addition of OA PA and Res Myo (Day 29). We thawed the PBMCs 18 h before co-culture and cultured them in RPMI medium containing 10% heat-inactivated fetal calf serum (FCS) and Pen-strep. Within this 18 h pre-incubation, PBMCs either incubated without any trigger or with 5 µg/ml lipopolysaccharide (LPS, eBioscience). Before adding them to the inner compartments of the trans-wells, we washed of the RPMI medium and re-suspended them in the respective HCM culture medium.

Live dyes

We incubated HLCs for 30 min with LipidSpot 488 and Mitotracker red staining to assess steatosis and mitochondrial membrane potential. We used all dyes according to manufacturer´s instructions. Specifically, Mitotracker red we used with a 200 nM end concentration. Eventually, we either performed live cell imaging or fixed cells in the culture plate using 4% paraformaldehyde with subsequent PBS washings before imaging.

RNA Isolation

We isolated RNA using a hybrid protocol of trizol RNA isolation combined with column-based purification (Qiagen or Thermo). We lysed cells in 1 ml of trizol (Thermo) to which we subsequently added 0.2 ml chloroform. All chloroform trizol mixtures then centrifuged for 10 min, using 12,000 g at 4°C. Then, we transferred the aqueous phase to a new tube and added 70% ethanol in a 1:1 ratio. This mixture we loaded on RNeasy Micro Kit columns (Qiagen). From this point we performed every step according to manufacturer´s recommendations (including the on-column DNAse treatment). We assessed the concentration of the isolated RNA using Nanodrop.

qPCR

For quantifying gene expression using qPCR, we reverse-transcribed RNA into cDNA using a cDNA Synthesis kit (High-Capacity cDNA Reverse Transcription Kit (Thermo, Cat. No. 4368813), biotechrabbitTM or Applied Biosystems™ High-Capacity RNA-to-cDNA™ Kit) according to manufacturer´s instructions. We then performed RT-qPCR using the PowerUp SYBR Green Master Mix (Applied Biosystems, Cat. No. A25776) on a QuantStudio 3 Real-Time PCR System (Thermo Fisher Scientific Inc.) according to the manufacturer's instructions. Primers were synthesized by Eurofins

Genomics, with sequences listed in Table 1. Gene expression changes were calculated using the ddCT method.

Table 1: Oligos used in this study

AFP_F	CCAGCTACCTGCCTTTCTGG
AFP_R	GGAGTGGGCTTTTTGTGTGC
CYP3A4_F	CCGAGTGGATTTCCTTCAGCTG
CYP3A4_R	TGCTCGTGGTTTCATAGCCAGC
RPS18_F	GCAGAATCCACGCCAGTACAAG
RPS18_R	GCTTGTTGTCCAGACCATTGGC

Measurement of the oxygen consumption rate

Cells were detached from one full 6-well plate and seeded on one full Geltrex (Thermo) coated Seahorse Plate on day 28 of HLC differentiation. For detachment, we washed HLCs with PBS and then incubated the cells for at least 10 min with 10x TrypLE (Gibco) until they rounded up. We added the 5-fold volume of PBS with 20% KO-Serum, centrifuged cells for 3 min using 200 g, and resuspended them in HCM complete media containing all supplements as described. We first added 50 µl of the cells for attachment, followed by 50 µl of more medium 5 h later. Then we exposed cells to 3 days of resistin, myostatin or both compared to the vehicle only, and measured oxygen consumption rate (OCR) using Seahorse Extracellular Flux (XF)-96 Bioanalyzer from Agilent Technologies as described previously (Kumar et al., 2024). Briefly, the XF basal medium from Agilent Technologies was supplemented with 10 mM glucose, 1 mM pyruvate, and 1 mM glutamine. The electron transport chain complexes inhibitors (oligomycin (2 µM), FCCP (1 µM), rotenone (1 µM), and antimycin (1 µM)) were titrated and delivered through injection at designated ports A, B, and C of the Bioanalyzer. The resulting data were then normalized to the protein content in each well.

RNA Sequencing

mRNA sequencing was performed at the BIH Genomics Core facility using Illumina sequencing and Illumina TruSeq stranded mRNA library preparation.

Features of the MASLD in vitro model dataset:

The MASLD in vitro model bulk rna-seq dataset consisted of 32 samples from two donor lines 1b and 5a (16 for each donor line, four of each sample), see Table 2.

Table 2 Sample conditions used for bulk RNA-sequencing and downstream analysis.

Name	Condition
HCM	healthy control (untreated cells)
OA PA	cells that were solely treated with an excess of free fatty acids
OA PA ResMyo	cells that in addition to free fatty acid excess also were exposed to 2 MASLD associated signaling molecules from other tissues (adipose and muscle tissue)
OA PA ResMyo PBMCs	cells that experienced both of the above mentioned conditions + a co-culture of stimulated

	primary immune cells (immune cells were not included in the RNA sequencing)

Processing and analysis of MASLD in vitro model RNA-seq dataset:

We started by carrying out a whole genome decoy-aware indexing and transcript quantification using Salmon v1.10.1 (Patro et al., 2017). The Salmon pipeline estimates transcript-level abundance from RNA-seq read data. We then used DESeq2 (Love et al., 2014), to test for differentially expressed genes between the following conditions:

I. OA PA vs HCM
II. OA PA ResMyo vs HCM
III. OA PA ResMyoPBMCs vs HCM

For each set of differentially expressed genes, we tested for enriched KEGG pathways (Kanehisa & Goto, 2000).

Imaging and image analysis

We imaged cells in their respective well plates using the Phenix High-Content Imaging system (Revity). We captured at least 10 individual images per well which we analyzed using the Signals Image Artist software (Version 1.3.29). For measuring steatosis or mitochondrial membrane potential, we manually set upper and lower thresholds for LipidSpot and Mitotracker staining in each experiment to eliminate background and artefacts. For Mitotracker staining we then measured intensity for the selected image region. To assess steatosis, we measured LipidSpot area and divided it by the respective Mitotracker area for each image. Respective signals for steatosis or Mitotracker we then further normalized as indicated.

Statistical testing

Data visualization and assessment of statistical significance we performed in RStudio or GraphPad Prism (Version 10). We used the statistical tests as indicated.

Results:

HLCs can model a spectral MASLD phenotype depending on injury hits

Steatosis is an unspecific hepatocyte response under multi-hit injury

Because MASLD models often only rely on single injuries like high concentrations of free fatty acids (Jeon et al., 2021; Ricchi et al., 2009), we cumulatively exposed HLCs to different MASLD-associated injuries, namely free fatty acid excess (OA/PA, 1 Hit), inter-organ signaling molecules (Res/Myo, 2 Hits) and inflammatory signaling (trans-well PBMC co-culture, 3 Hits)**(Fig. 1A)**. First, we optimized the maturation of HLCs using a combination of T3, NaSe, and CDCA, assessed *via* gene expression **(Sup. Fig. 1A)**. Then, we evaluated the MASLD hallmark steatosis in HLCs exposed to different MASLD injury types. We tested this for HLCs derived from one donor line with the MASLD-associated homozygous mutation in the PNPLA3 gene (PNPLA3-I148M) or one without any MASLD-associated pre-disposition (PNPLA3-wt). The 3-day exposure to OA and PA clearly elevated lipid droplet area in both tested donor cell line derived HLCs **(Fig. 1B and C)**. Neither the addition of the MALSD-associated resistin and myostatin, nor the trans-well co-culture with primary immune cells significantly aggravated steatosis levels compared to OA/PA. Moreover, the PNPLA3-I148M-donor HLCs tended to have higher steatosis at injury conditions compared to the PNPLA3-wildtype donor HLCs (p-value 0.047, wilcoxon test of all

injury conditions between PNPLA3-wt and PNPLA3-I148M). Given the generic steatosis response to OA/PA, we proceeded to assessing nuanced injury hallmarks.

Functional mitochondrial dynamics in HLCs respond to multi-hit impairment

Another hallmark of MASLD is perturbed mitochondrial health (Fromenty & Roden, 2023). In our model, mitochondrial morphology seemed altered the more injury hits we added **(Fig. 1B)**. In contrast, in healthy cells, mitochondrial signal spreads out evenly over the cells, in cumulative injury, this changes to a more granular-like phenotype with some bright spots and more centered and a decreased signal in outer cell areas. Interestingly, only the co-culture with non-stimulated PBMCs significantly reduced mitochondrial membrane potential in the PNPLA3-wt donor HLCs. For the PNPLA3-I148M donor HLCs, the combination of Res and Myo with OA/PA significantly reduced membrane potential, further aggravated when combined with PBMC co-culture. This indicates a higher susceptibility of the PNPLA3-I148M donor line for mitochondrial membrane potential alterations by Res and Myo. To further understand the impact of Res and Myo on mitochondria, we exposed HLCs to each factor individually or combined without further injury in the PNPLA3-I148M line. Both individually and combined significantly decreased Mitotracker signal in HLCs **(Sup. Fig. 1B)**. Further, both combined significantly reduced mitochondrial spare respiratory capacity **(Sup. Fig. 1C)**. On the same note, we further explored the PBMC-to-HLC-mitochondria axis by assessing the expression of the mitochondrial biogenesis master regulator *PPARGC1A* under different conditions. We found that *PPARGC1A* expression was significantly downregulated in HLCs co-cultured with PBMCs in combination with other disease hits **(Sup. Fig. 1D)**, but not when PBMCs were present alone or when other disease hits were applied without PBMCs **(Sup. Fig. 1E)**. PBMCs pre-stimulated with LPS for 18h seemed adding to this effect **(Sup. Fig. 1D)**. This indicates inherent triggers of the disease model for factor secretion in PBMCs that affect expression of mitochondrial genes in HLCs. Adding pro-inflammatory PBMCs may thereby further exacerbate this effect. Thus, we concluded to use pre-stimulated PBMCs in follow-up experiments for more severe MASH modeling. This is also in accordance with TNFa and IL1B being highly associated with MASH, and secreted in LPS-stimulated PBMCs (Duan et al., 2022; Janský et al., 2003).

Transcriptomic signatures reveal compounded response to cumulative injuries

To further understand differences in respective injury hits at the molecular level, we performed bulk RNA sequencing for each injury condition and untreated cells, including both donor lines. First, we observed clear differences between individual HLC differentiations on the transcriptomic level **(Sup. Fig. 2A&B)**. This was more elevated in the PNPLA3-I148M donor line than in the PNPLA3-wt donor line. However, the cumulative addition of injury hits led to an increased clustering intra-differentiation distance and accumulative increase of differentially expressed genes (DEGs) in both donor lines **(Sup. Fig. 2C&D and Fig. 1E)**. Finally, we performed an integrative injury analysis by combining metrics of steatosis, mitochondrial membrane potential, and DEG alterations to derive an overall MASLD injury score **(Fig. 1F)**. We normalized data to PNPLA3-wt HLCs, with untreated cells representing 0% injury and cells exposed to all three stressors representing 100%. While PNPLA3-wt HLCs seem to exhibit a compounded injury response, the PNPLA3-I148M line reached a higher overall injury score earlier in the exposure process. Our results show how the cumulative exposure to MASLD injury progressively elevates MASLD-related injury in HLCs. Also, clear inter-donor effects were visible, as here described for PNPLA3-wt vs PNPLA3-I148M donor lines.

Transcriptomic data reveals inflammatory reprogramming and loss of nuclear encoded mitochondrial metabolism

To further understand the mechanisms in respective injury hits in an unbiased manner, we performed an enrichment analysis of Kyoto Encyclopedia of Genes and Genomes (KEGG) pathways **(Fig. 2A)**. We hereby focused on the two-hit and three-hit model in PNPLA3-wt HLCs, since other conditions did not show sufficient statistical power due to the inter-differentiation differences **(Sup. Fig 2A&B)**. HLCs exposed to free fatty acid excess plus resistin and myostatin showed primarily changes in the cytoskeleton as well as, for example, focal adhesion and ECM interactions. Interestingly, we found proteoglycans in cancer significantly enriched. Similar KEGG pathways were affected for HLCs exposed to the 3-Hit model, including PBMCs. However, in these conditions many inflammatory KEGG pathways such as IL-17, TNFa or NF-kB signaling showed an enrichment, indicating that we here model a more advanced stage of the disease, namely MASH. In both the two-hit and three-hit model, the down-regulated genes were enriched for metabolic KEGG pathways, indicating metabolic impairment in HLCs. Next, we hypothesized that the expression of mitochondria-associated genes is impacted differentially by the respective MASLD model, similar to the in vivo situation (Fromenty & Roden, 2023). To evaluate this hypothesis, we filtered all DEGs for genes with proteins located at the mitochondrion based on MitoCarta 3.0 (Rath et al., 2021). Again, along the cumulative addition of hits an increased number of mitochondria-associated genes were down-regulated in HLCs **(Fig. 2B)**. The few up-regulated genes covered for example *UCP2*, which is a mitochondrial uncoupling protein involved in membrane potential loss, supporting the Mitotracker-based data. We went on to look at the expression levels of the OXPHOS genes along the different injury hits **(Fig. 2C)**. We saw an overall incline in OXPHOS gene expression, being present already at the stage of Res and Myo addition, most pronounced in PBMC co-culture conditions. In sum, transcriptomic analysis supported the cumulative aggravation of our MASLD-to-MASH model, which is suited to evaluate potential drug candidates in a stage-specific manner.

Discussion:

In this study, we present an iPSC-derived multi-hit model that captures the progression from MASLD to MASH, allowing us to explore the complex pathophysiology involved. Our modular approach allows for a representation of disease progression in vitro, facilitating testing stage-specific therapeutic interventions. Common iPSC-based MASLD models typically involve short-term exposure to free fatty acids (Rezvani et al., 2023). To enhance the physiological relevance of pre-clinical models, we incorporated a more nuanced cocktail of MASLD-associated factors, such as resistin and myostatin, and PBMC co-culture. Our data suggests that steatotic (per OA addition) and lipotoxic (per PA addition) burden leads to an adaptive response of the hepatocytes, with critical transition points when Res/Myo and PBMC-coculture were added. This indicates that in our model, not substrate excess per se but the signaling from multiple tissues or cell types drives significant changes. This is of particular interest since the role of Res and Myo in MASLD development still needs to be resolved, especially in a physiological human context. For example, the contrasting roles of Res in human and mouse systems is still a matter of debate, not only for liver biology (Acquarone et al., 2019). Assessing these factors in physiological human systems, such as human iPSC-derived hepatocytes, makes it increasingly relevant. The mitochondrial effect of Res we observed was also reported in mice and carcinoma cell lines (Wen et al., 2021; Yang et al., 2023; Zhou et al., 2013). Myo today has not been intensively tested in human physiological hepatocyte models. In mouse hepatocytes and cancer cells it increased triglyceride content (X. Liu et al., 2019) or impacted mitochondria (Y. Liu et al., 2013), respectively. Even though not directly assessed for steatosis, Myo, like Res, also impacted mitochondrial dynamics in our model. Thus, our findings from a physiological human system support the mitochondrial entanglement of Res and Myo. However, such effects were pronounced differently between both donor lines. Whereas in the PNPLA3-wt donor morphology alterations and gene expression changes were observed, the PNPLA3-I148M also experienced a loss of mitochondrial membrane potential. These findings showcase donor-dependent variability in cellular models.

The functional implications of HLC-leukocyte co-cultures have been shown recently for insulin resistance modeling using iPSC-derived macrophages (Groeger et al., 2023). Since MASH follows MASLD by bone marrow-derived cells interacting with the liver, including a multitude of infiltrating leukocytes, we here reasoned to add PBMCs after pre-stressing HLCs. The addition of PBMCs in trans-well inserts proved feasible, as these remained >90% viable after co-culture (assessed via TrypanBlue staining). Experiments with co-cultured patient-derived PBMCs would allow us to test if the source of the donor PBMCs or the hepatic environment promotes the disease phenotype. However, as shown in the *PPARGC1A* expression data, the applied disease model already triggers specific factor secretion in co-cultured PBMCs inherently. A limitation of this approach is the lack of direct cell contact, which could be ideally facilitated in autologous co-cultures. However, establishing and scaling these co-cultures logistically is difficult. Further, characterizing the PBMC compartment and the crosstalk happening in a two-sided manner in respective co-cultures would complete the picture, which was, however, out of the scope of this manuscript.

Also, the here described impact of genetic background displays the potential iPSC-derived systems offer. Either by combining this modular in vitro MASLD progression with strong-powered multi-donor analysis as shown by Kimura et al (Kimura et al., 2022) or by precise pooled genetic testing using isogenic backgrounds. Thus, extending the applicability of described platforms. Especially since the multi-hit permissiveness can be different depending on respective individuals, as also proposed by our work. Thus, testing respective hits in different genetic backgrounds will aid to further understand disease processes.

To conclude, we here model the compounded effects of different MASLD injuries, including extra-hepatic signaling and inflammation. This model will be used to test stage-specific disease interception with candidate anti-MASLD factors. Further studies will explore more facets of the here-described system.

Limitations:

This study has the following limitations. First, we experienced inter-differentiation differences on a transcriptomic level, limiting the sensitivity for detecting disease-specific DEGs. Since these differences were bigger for the PNPLA3-I148M line, probably fewer DEGs were detected. A bigger sample size would help circumvent this. Further, we thus far tested only one PBMC donor. Increasing the biological sample size will help identify inter-donor differences if present. Additionally, a deeper characterization of the PBMCs and viability will provide a deeper understanding of the disease model described here. Further, we did not have isogenic controls for the PNPLA3-I148M mediated effects, restricting us and the reader from seeing respective effects only descriptively. Eventually, more comprehensive Seahorse assays will help to understand mitochondrial alterations in detail. However, these proved technically challenging to detect nuanced differences in iPSC-derived hepatocytes and need further optimization.

Figure Legends

Figure 1: Modeling the multifactorial MASLD progression in hepatocyte-like cells A) Schematic of the multi-hit MASLD model in iPSC-derived hepatocytes and respective injury trajectories. **B)** Representative fluorescence microscopic images of HLCs cumulatively exposed to Oleic Acid and Palmitic Acid (OA/PA), Resistin and Myostatin (Res/Myo) and peripheral blood mono-nuclear cells (PBMCs) indicated as respective injury hit models and stained with LipidSpot and Mitotracker Red. **C)** Quantification of steatotic area normalized to respective Mitotracker area in percent. Dots represent independent wells. Tukey-Post Hoc analysis to test for significance. **D)** Quantification of Mitotracker signal intensity, normalized to untreated cells. Dots represent independent wells. Wilcoxon test to test for significance. **E)** Number of differentially expressed genes from bulk RNAsequencing in different injury conditions compared to untreated cells **F)** Pooled injury curve fits including the scaled injury

parameters steatosis, mitochondrial membrane potential alterations and number of DEGs from RNA sequencing. Injury scores were normalized to PNPLA3-wt conditions for which no hits represented 0% and all hits represent 100%.

Figure 2: Transcriptomic data reveals inflammatory reprogramming and loss of genomically encoded mitochondrial metabolism A) Enriched and reduced Kyoto Encyclopedia of Genes and Genomes (KEGG) pathways for the two hit MASLD model including OA/PA and Res/Myo as well as the three hit model including in addition pro-inflammatory PBMCs. **B)** DEGs of respective two and three-hit models filtered for genes located at the mitochondria, based on their inclusion in MitoCarta3.0. **C)** Relative expression levels of genes involved in oxidative phosphorylation for two independent differentiations of HLCs.

Supplementary Figure 1: Hepatocyte response to maturation and metabolic stimuli: A) Gene expression levels of the hepatocyte maturity and fetal marker *CYP3A4* (left) and *AFP* (right), respectively, in HLCs after treatment with either T3/NaSe, CDCA or both. Fold changes were normalized to the untreated cells. Dots represent independent wells. One-Way ANOVA with tukey post-hoc was used for assessing statistical significance. **B)** Mitochondrial membrane potential assessed using mitotracker after treatment with either resistin, myostatin or both. Signals were normalized to the untreated control. **C)** SeaHorse parameter for HLCs treated either resistin, myostatin or both. Signals were normalized to protein content. **D)** Gene expression levels of PPARGC1A in HLCs exposed to different PBMC co-culture conditions, normalized to untreated cells. Dots represent independent wells. Significance was assessed using one-way anova with Tukey-Post Hoc. *$p<0.05$, **$p<0.01$, ***$p<0.001$. **E)** Gene expression levels of PPARGC1A in HLCs exposed to OA/PA or OA/PA with Res/Myo. Gene expression levels were normalized to the untreated control.

Supplementary Figure 2: Global transcriptomic changes in HLCs exposed to cumulative injury: PCA plots of transcriptomes from HLCs derived from the PNPLA3-wt **(A)** or -I148M **(B)** donor. Colors indicate either injury type or differentiation. **C)** Volcano plot of DEGs in PNPLA3-wt or PNPLA3-I148M HLCs exposed to different injuries. All shown dots are statistically significant genes, the highest are marked in red or blue.

Acknowledgement:

The authors of this scientific article would like to acknowledge the funding provided by the Deutsche Forschungsgemeinschaft (DFG) Emmy Noether Programme to M. R. (RE 3749/2-1) and the Young Investigator Award awarded by Charite 3R to J.W. We thank the members of the BIH Core Unit pluripotent Stem cells and Organoids, specifically Valeria Fernandez Vallone, Janine Cernoch and Claudia Schaar for their technical support. We also thank Janine Altmüller and Tatiana Borodina of the MDC/BIH Genomics Platform, Berlin for technical support. In addition, we would like to thank the HPC for Research/Clinic cluster of the Berlin Institute of Health for data storage.

We are also grateful for the support provided by all the current and former members of the Rezvani Lab, specifically Natalia Martagón Calderón and Reinhild Dünnebacke. We would also like to thank the following people for sharing their expertise: Amr Al Shebel, Tilman Breiderhoff, Kerstin Sommer, Sandra Gerstenberg, Verena Klämbt, Marah Alhabahbeh, Christian Hudert, Adrien Guillot, Hanyang Liu, Tian Lan, Guo Yin and Frank Tacke. Further, we want to thank Aras Mattis from the University of California San Francisco for sharing expertise.

References:

Acquarone, E., Monacelli, F., Borghi, R., Nencioni, A., & Odetti, P. (2019). Resistin: A reappraisal. *Mechanisms of Ageing and Development*, *178*, 46–63. https://doi.org/10.1016/j.mad.2019.01.004

Ajmera, V., Perito, E. R., Bass, N. M., Terrault, N. A., Yates, K. P., Gill, R., Loomba, R., Diehl, A. M., Aouizerat, B. E., & for the NASH Clinical Research Network. (2017). Novel plasma biomarkers associated with liver disease severity in adults with nonalcoholic fatty liver disease. *Hepatology*, *65*(1), 65–77. https://doi.org/10.1002/hep.28776

Bjørndal, B., Alterås, E. K., Lindquist, C., Svardal, A., Skorve, J., & Berge, R. K. (2018). Associations between fatty acid oxidation, hepatic mitochondrial function, and plasma acylcarnitine levels in mice. *Nutrition & Metabolism*, *15*(1), 10. https://doi.org/10.1186/s12986-018-0241-7

Buzzetti, E., Pinzani, M., & Tsochatzis, E. A. (2016). The multiple-hit pathogenesis of non-alcoholic fatty liver disease (NAFLD). *Metabolism*, *65*(8), 1038–1048. https://doi.org/10.1016/j.metabol.2015.12.012

Chandak, P., Huang, K., & Zitnik, M. (2023). Building a knowledge graph to enable precision medicine. *Scientific Data*, *10*(1), 67. https://doi.org/10.1038/s41597-023-01960-3

Cheng, F., Kovács, I. A., & Barabási, A.-L. (2019). Network-based prediction of drug combinations. *Nature Communications*, *10*(1), 1197. https://doi.org/10.1038/s41467-019-09186-x

Delogu, W., Caligiuri, A., Provenzano, A., Rosso, C., Bugianesi, E., Coratti, A., Macias-Barragan, J., Galastri, S., Di Maira, G., & Marra, F. (2019). Myostatin regulates the fibrogenic phenotype of hepatic stellate cells via c-jun N-terminal kinase activation. *Digestive and Liver Disease*, *51*(10), 1400–1408. https://doi.org/10.1016/j.dld.2019.03.002

Duan, Y., Pan, X., Luo, J., Xiao, X., Li, J., Bestman, P. L., & Luo, M. (2022). Association of Inflammatory Cytokines With Non-Alcoholic Fatty Liver Disease. *Frontiers in Immunology*, *13*, 880298. https://doi.org/10.3389/fimmu.2022.880298

Ferraioli, G., & Monteiro, L. B. S. (2019). Ultrasound-based techniques for the diagnosis of liver steatosis. *World Journal of Gastroenterology*, *25*(40), 6053–6062. https://doi.org/10.3748/wjg.v25.i40.6053

Fromenty, B., & Roden, M. (2023). Mitochondrial alterations in fatty liver diseases. *Journal of Hepatology*, *78*(2), 415–429. https://doi.org/10.1016/j.jhep.2022.09.020

García, P. S., Cabbabe, A., Kambadur, R., Nicholas, G., & Csete, M. (2010). Elevated Myostatin Levels in Patients with Liver Disease: A Potential Contributor to Skeletal Muscle Wasting. *Anesthesia & Analgesia*, *111*(3), 707–709. https://doi.org/10.1213/ANE.0b013e3181eac1c9

Govaere, O., Cockell, S., Tiniakos, D., Queen, R., Younes, R., Vacca, M., Alexander, L., Ravaioli, F., Palmer, J., Petta, S., Boursier, J., Rosso, C., Johnson, K., Wonders, K., Day, C. P., Ekstedt, M., Orešič, M., Darlay, R., Cordell, H. J., … Anstee, Q. M. (2020). Transcriptomic profiling across the nonalcoholic fatty liver disease spectrum reveals gene signatures for steatohepatitis and fibrosis. *Science Translational Medicine*, *12*(572), eaba4448. https://doi.org/10.1126/scitranslmed.aba4448

Groeger, M., Matsuo, K., Heidary Arash, E., Pereira, A., Le Guillou, D., Pino, C., Telles-Silva, K. A., Maher, J. J., Hsiao, E. C., & Willenbring, H. (2023). Modeling and therapeutic targeting of inflammation-induced hepatic insulin resistance using human iPSC-derived hepatocytes and macrophages. *Nature Communications*, *14*(1), 3902. https://doi.org/10.1038/s41467-023-39311-w

Guney, E., Menche, J., Vidal, M., & Barábasi, A.-L. (2016). Network-based in silico drug efficacy screening. *Nature Communications*, *7*, 10331. https://doi.org/10.1038/ncomms10331

Han, N., Hwang, W., Tzelepis, K., Schmerer, P., Yankova, E., MacMahon, M., Lei, W., M Katritsis, N., Liu, A., Felgenhauer, U., Schuldt, A., Harris, R., Chapman, K., McCaughan, F., Weber, F., & Kouzarides, T. (2021). Identification of SARS-CoV-2-induced pathways reveals drug repurposing strategies. *Science Advances*, *7*(27), eabh3032. https://doi.org/10.1126/sciadv.abh3032

Janský, L., Reymanová, P., & Kopecký, J. (2003). Dynamics of cytokine production in human peripheral blood mononuclear cells stimulated by LPS or infected by Borrelia. *Physiological Research*, *52*(6), 593–598.

Jeon, J., Lee, S. H., Kim, D., & Sung, J. H. (2021). In vitro hepatic steatosis model based on gut–liver-on-a-chip. *Biotechnology Progress*, *37*(3), e3121. https://doi.org/10.1002/btpr.3121

Kajiwara, M., Aoi, T., Okita, K., Takahashi, R., Inoue, H., Takayama, N., Endo, H., Eto, K., Toguchida, J., Uemoto, S., & Yamanaka, S. (2012). Donor-dependent variations in hepatic differentiation from human-induced pluripotent stem cells. *Proceedings of the National Academy of Sciences*, *109*(31), 12538–12543. https://doi.org/10.1073/pnas.1209979109

Kanehisa, M., & Goto, S. (2000). KEGG: Kyoto encyclopedia of genes and genomes. *Nucleic Acids Research*, *28*(1), 27–30. https://doi.org/10.1093/nar/28.1.27

Kimura, M., Iguchi, T., Iwasawa, K., Dunn, A., Thompson, W. L., Yoneyama, Y., Chaturvedi, P., Zorn, A. M., Wintzinger, M., Quattrocelli, M., Watanabe-Chailland, M., Zhu, G., Fujimoto, M., Kumbaji, M., Kodaka, A., Gindin, Y., Chung, C., Myers, R. P., Subramanian, G. M., … Takebe, T. (2022). En masse organoid phenotyping informs metabolic-associated genetic susceptibility to NASH. *Cell*, *185*(22), 4216-4232.e16. https://doi.org/10.1016/j.cell.2022.09.031

Kumar, P., Hassan, M., Tacke, F., & Engelmann, C. (2024). Delineating the heterogeneity of senescence-induced-functional alterations in hepatocytes. *Cellular and Molecular Life Sciences*, *81*(1), 200. https://doi.org/10.1007/s00018-024-05230-2

Langfelder, P., & Horvath, S. (2008). WGCNA: An R package for weighted correlation network analysis. *BMC Bioinformatics*, *9*, 559. https://doi.org/10.1186/1471-2105-9-559

Li, X., & Wang, H. (2020). Multiple organs involved in the pathogenesis of non-alcoholic fatty liver disease. *Cell & Bioscience*, *10*(1), 140. https://doi.org/10.1186/s13578-020-00507-y

Liu, X., Pan, J. P., Bauman, W. A., & Cardozo, C. P. (2019). AdipoRon prevents myostatin-induced upregulation of fatty acid synthesis and downregulation of insulin activity in a mouse hepatocyte line. *Physiological Reports*, *7*(13). https://doi.org/10.14814/phy2.14152

Liu, Y., Cheng, H., Zhou, Y., Zhu, Y., Bian, R., Chen, Y., Li, C., Ma, Q., Zheng, Q., Zhang, Y., Jin, H., Wang, X., Chen, Q., & Zhu, D. (2013). Myostatin induces mitochondrial metabolic alteration and typical apoptosis in cancer cells. *Cell Death & Disease*, *4*(2), e494–e494. https://doi.org/10.1038/cddis.2013.31

Love, M. I., Huber, W., & Anders, S. (2014). Moderated estimation of fold change and dispersion for RNA-seq data with DESeq2. *Genome Biology*, *15*(12), 550. https://doi.org/10.1186/s13059-014-0550-8

Ma, H., De Zwaan, E., Guo, Y. E., Cejas, P., Thiru, P., Van De Bunt, M., Jeppesen, J. F., Syamala, S., Dall'Agnese, A., Abraham, B. J., Fu, D., Garrett-Engele, C., Lee, T. I., Long, H. W., Griffith, L. G., Young, R. A., & Jaenisch, R. (2022). The nuclear receptor THRB facilitates differentiation of human PSCs into more mature hepatocytes. *Cell Stem Cell*, *29*(5), 795-809.e11. https://doi.org/10.1016/j.stem.2022.03.015

Mendez, D., Gaulton, A., Bento, A. P., Chambers, J., De Veij, M., Félix, E., Magariños, M. P., Mosquera, J. F., Mutowo, P., Nowotka, M., Gordillo-Marañón, M., Hunter, F., Junco, L., Mugumbate, G., Rodriguez-Lopez, M., Atkinson, F., Bosc, N., Radoux, C. J., Segura-Cabrera, A., … Leach, A. R. (2019). ChEMBL: Towards direct deposition of bioassay data. *Nucleic Acids Research*, *47*(D1), D930–D940. https://doi.org/10.1093/nar/gky1075

Myint, M., Oppedisano, F., De Giorgi, V., Kim, B.-M., Marincola, F. M., Alter, H. J., & Nesci, S. (2023). Inflammatory signaling in NASH driven by hepatocyte mitochondrial dysfunctions. *Journal of Translational Medicine*, *21*(1), 757. https://doi.org/10.1186/s12967-023-04627-0

Nell, P., Kattler, K., Feuerborn, D., Hellwig, B., Rieck, A., Salhab, A., Lepikhov, K., Gasparoni, G., Thomitzek, A., Belgasmi, K., Blüthgen, N., Morkel, M., Küppers-Munther, B., Godoy, P., Hay, D. C., Cadenas, C., Marchan, R., Vartak, N., Edlund, K., … Hengstler, J. G. (2022). Identification of an FXR-modulated liver-intestine hybrid state in iPSC-derived hepatocyte-like cells. *Journal of Hepatology*, *77*(5), 1386–1398. https://doi.org/10.1016/j.jhep.2022.07.009

Park, K., Gooz, M., Ye, Z., Zhang, J., Beeson, G. C., Rockey, D. C., & Kim, S. (2021). Flavin Adenine Dinucleotide Depletion Caused by electron transfer flavoprotein subunit alpha Haploinsufficiency Leads to Hepatic Steatosis and Injury in Zebrafish. *Hepatology Communications*, *5*(6), 976–991. https://doi.org/10.1002/hep4.1691

Patro, R., Duggal, G., Love, M. I., Irizarry, R. A., & Kingsford, C. (2017). Salmon provides fast and bias-aware quantification of transcript expression. *Nature Methods*, *14*(4), 417–419. https://doi.org/10.1038/nmeth.4197

Rath, S., Sharma, R., Gupta, R., Ast, T., Chan, C., Durham, T. J., Goodman, R. P., Grabarek, Z., Haas, M. E., Hung, W. H. W., Joshi, P. R., Jourdain, A. A., Kim, S. H., Kotrys, A. V., Lam, S. S., McCoy, J. G., Meisel, J. D., Miranda, M., Panda, A., … Mootha, V. K. (2021). MitoCarta3.0: An updated mitochondrial proteome now with sub-organelle localization and pathway annotations. *Nucleic Acids Research*, *49*(D1), D1541–D1547. https://doi.org/10.1093/nar/gkaa1011

Rezvani, M., Vallier, L., & Guillot, A. (2023). Modeling Nonalcoholic Fatty Liver Disease in the Dish Using Human-Specific Platforms: Strategies and Limitations. *Cellular and Molecular Gastroenterology and Hepatology*, *15*(5), 1135–1145. https://doi.org/10.1016/j.jcmgh.2023.01.014

Ricchi, M., Odoardi, M. R., Carulli, L., Anzivino, C., Ballestri, S., Pinetti, A., Fantoni, L. I., Marra, F., Bertolotti, M., Banni, S., Lonardo, A., Carulli, N., & Loria, P. (2009). Differential effect of oleic and palmitic acid on lipid accumulation and apoptosis in cultured hepatocytes. *Journal of Gastroenterology and Hepatology*, *24*(5), 830–840. https://doi.org/10.1111/j.1440-1746.2008.05733.x

Szklarczyk, D., Kirsch, R., Koutrouli, M., Nastou, K., Mehryary, F., Hachilif, R., Gable, A. L., Fang, T., Doncheva, N. T., Pyysalo, S., Bork, P., Jensen, L. J., & von Mering, C. (2023). The STRING database in 2023: Protein-protein association networks and functional enrichment analyses for any sequenced genome of interest. *Nucleic Acids Research*, *51*(D1), D638–D646. https://doi.org/10.1093/nar/gkac1000

Szklarczyk, D., Santos, A., von Mering, C., Jensen, L. J., Bork, P., & Kuhn, M. (2016). STITCH 5: Augmenting protein-chemical interaction networks with tissue and affinity data. *Nucleic Acids Research*, *44*(D1), D380-384. https://doi.org/10.1093/nar/gkv1277

Tang, J., Hegeman, M. A., Hu, J., Xie, M., Shi, W., Jiang, Y., De Boer, V., Guo, Y., Hou, S., & Keijer, J. (2017). Severe riboflavin deficiency induces alterations in the hepatic proteome of starter

Pekin ducks. *British Journal of Nutrition*, *118*(9), 641–650. https://doi.org/10.1017/S0007114517002641

Tang, N., Hong, F., Hao, W., Yu, T.-T., Wang, G.-G., & Li, W. (2022). Riboflavin ameliorates mitochondrial dysfunction via the AMPK/PGC1α/HO-1 signaling pathway and attenuates carbon tetrachloride-induced liver fibrosis in rats. *Experimental and Therapeutic Medicine*, *24*(4), 608. https://doi.org/10.3892/etm.2022.11545

Tilson, S. G., Morell, C. M., Lenaerts, A., Park, S. B., Hu, Z., Jenkins, B., Koulman, A., Liang, T. J., & Vallier, L. (2021). Modeling PNPLA3-Associated NAFLD Using Human-Induced Pluripotent Stem Cells. *Hepatology*, *74*(6), 2998–3017. https://doi.org/10.1002/hep.32063

Wang, Y., Bian, X., Wan, M., Dong, W., Gao, W., Yao, Z., & Guo, C. (2024). Effects of riboflavin deficiency and high dietary fat on hepatic lipid accumulation: A synergetic action in the development of non-alcoholic fatty liver disease. *Nutrition & Metabolism*, *21*(1), 1. https://doi.org/10.1186/s12986-023-00775-8

Wen, F., Shi, Z., Liu, X., Tan, Y., Wei, L., Zhu, X., Zhang, H., Zhu, X., Meng, X., Ji, W., Yang, M., & Lu, Z. (2021). Acute Elevated Resistin Exacerbates Mitochondrial Damage and Aggravates Liver Steatosis Through AMPK/PGC-1α Signaling Pathway in Male NAFLD Mice. *Hormone and Metabolic Research*, *53*(02), 132–144. https://doi.org/10.1055/a-1293-8250

Wilkes, J. J., Lloyd, D. J., & Gekakis, N. (2009). Loss-of-Function Mutation in Myostatin Reduces Tumor Necrosis Factor α Production and Protects Liver Against Obesity-Induced Insulin Resistance. *Diabetes*, *58*(5), 1133–1143. https://doi.org/10.2337/db08-0245

Wishart, D. S., Feunang, Y. D., Guo, A. C., Lo, E. J., Marcu, A., Grant, J. R., Sajed, T., Johnson, D., Li, C., Sayeeda, Z., Assempour, N., Iynkkaran, I., Liu, Y., Maciejewski, A., Gale, N., Wilson, A., Chin, L., Cummings, R., Le, D., … Wilson, M. (2018). DrugBank 5.0: A major update to the DrugBank database for 2018. *Nucleic Acids Research*, *46*(D1), D1074–D1082. https://doi.org/10.1093/nar/gkx1037

Xu, Q., Cao, Y., Zhong, X., Qin, X., Feng, J., Peng, H., Su, Y., Ma, Z., & Zhou, S. (2023). Riboflavin protects against heart failure via SCAD-dependent DJ-1–Keap1–Nrf2 signalling pathway. *British Journal of Pharmacology*, *180*(23), 3024–3044. https://doi.org/10.1111/bph.16184

Yang, H.-M., Kim, J., Shin, D., Kim, J.-Y., You, J., Lee, H.-C., Jang, H.-D., & Kim, H.-S. (2023). Resistin impairs mitochondrial homeostasis via cyclase-associated protein 1-mediated fission, leading to obesity-induced metabolic diseases. *Metabolism*, *138*, 155343. https://doi.org/10.1016/j.metabol.2022.155343

Younossi, Z. M., Golabi, P., Paik, J. M., Henry, A., Van Dongen, C., & Henry, L. (2023). The global epidemiology of nonalcoholic fatty liver disease (NAFLD) and nonalcoholic steatohepatitis (NASH): A systematic review. *Hepatology*, *77*(4), 1335–1347. https://doi.org/10.1097/HEP.0000000000000004

Zhang, B., & Horvath, S. (2005). A general framework for weighted gene co-expression network analysis. *Statistical Applications in Genetics and Molecular Biology*, *4*, Article17. https://doi.org/10.2202/1544-6115.1128

Zhang, D., Zhou, D., Wang, X., Li, M., Zhang, J., He, N., Zhou, X., Li, Z., Huang, G., Li, W., & Qian, Z. (2024). Selenium and vitamin B_2 cosupplementation alleviates high-fat-diet-induced nonalcoholic fatty liver disease in rats by regulating hepatic lipid metabolism. *European Journal of Lipid Science and Technology*, *126*(1), 2300020. https://doi.org/10.1002/ejlt.202300020

Zhou, L., Yu, X., Meng, Q., Li, H., Niu, C., Jiang, Y., Cai, Y., Li, M., Li, Q., An, C., Shu, L., Chen, A., Su, H., Tang, Y., Yin, S., Raschke, S., Eckardt, K., Eckel, J., & Yang, Z. (2013). Resistin reduces mitochondria and induces hepatic steatosis in mice by the protein kinase C/protein kinase G/p65/PPAR gamma coactivator 1 alpha pathway. *Hepatology*, *57*(4), 1384–1393. https://doi.org/10.1002/hep.26167

Figure 1: Modeling the multifactorial MASLD progression in hepatocyte-like cells

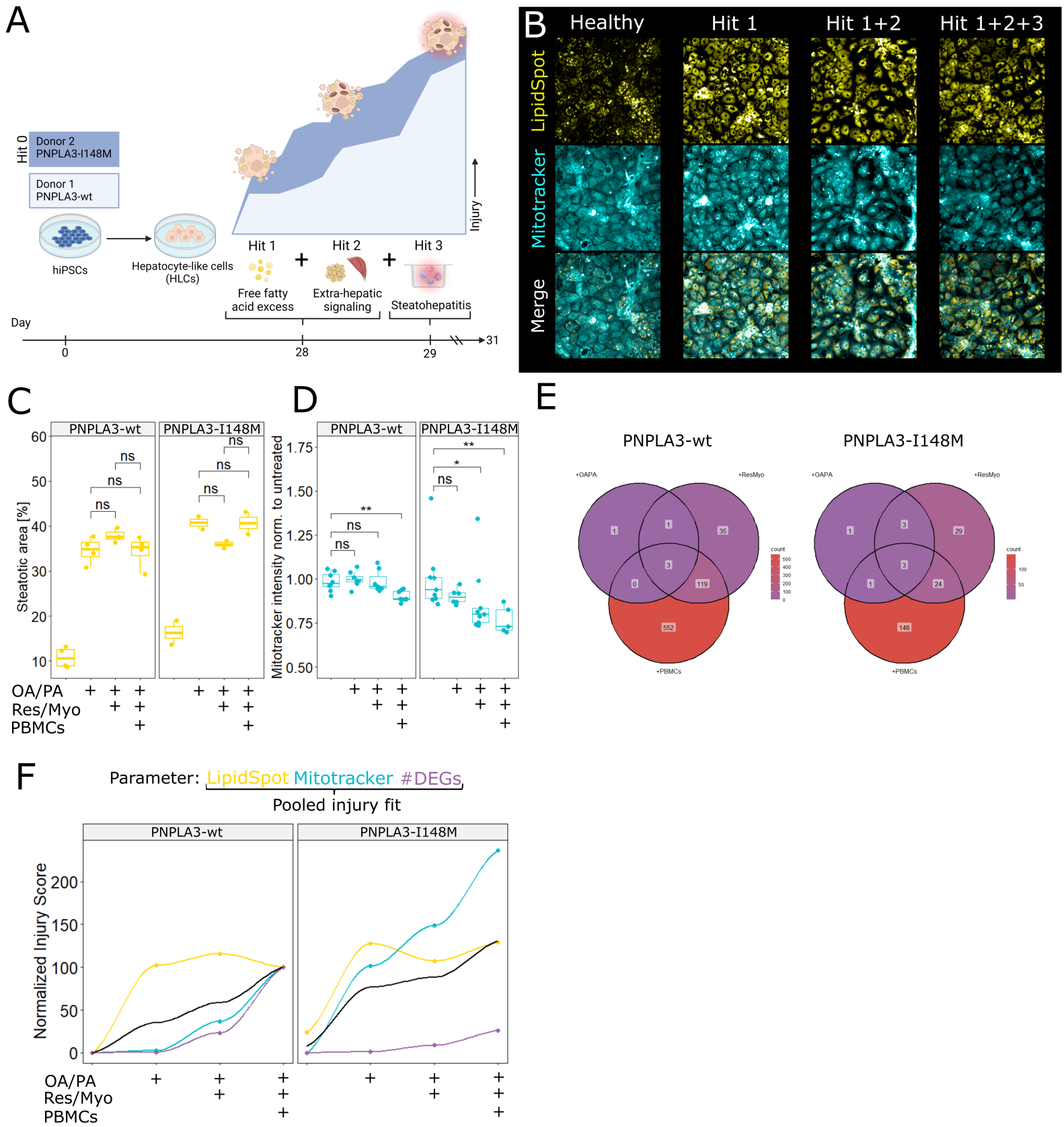

Figure 2: Transcriptomic data reveals inflammatory reprogramming and loss of genomically encoded mitochondrial metabolism

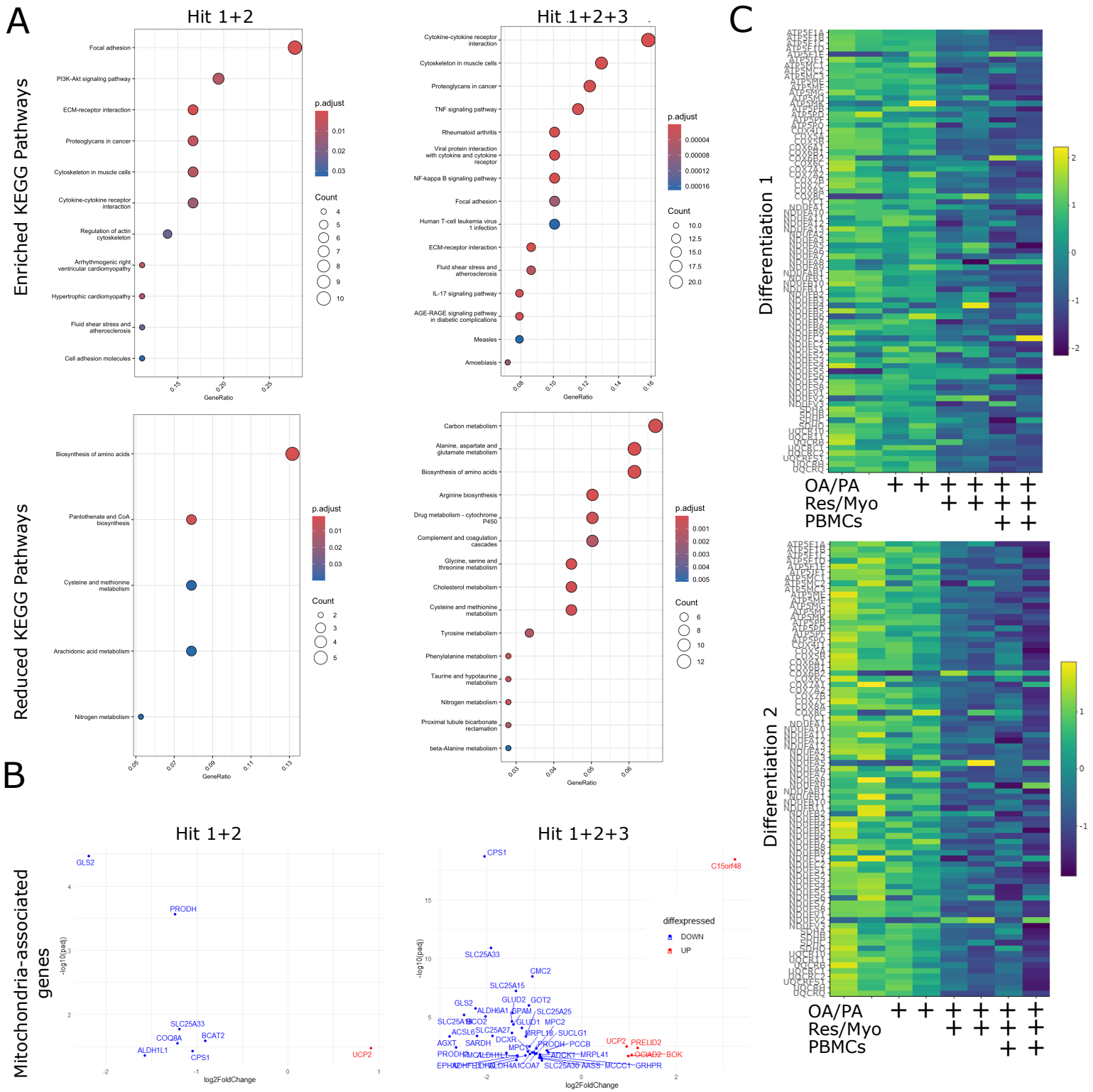

Supp. Figure 1: Hepatocyte response to maturation and metabolic stimuli

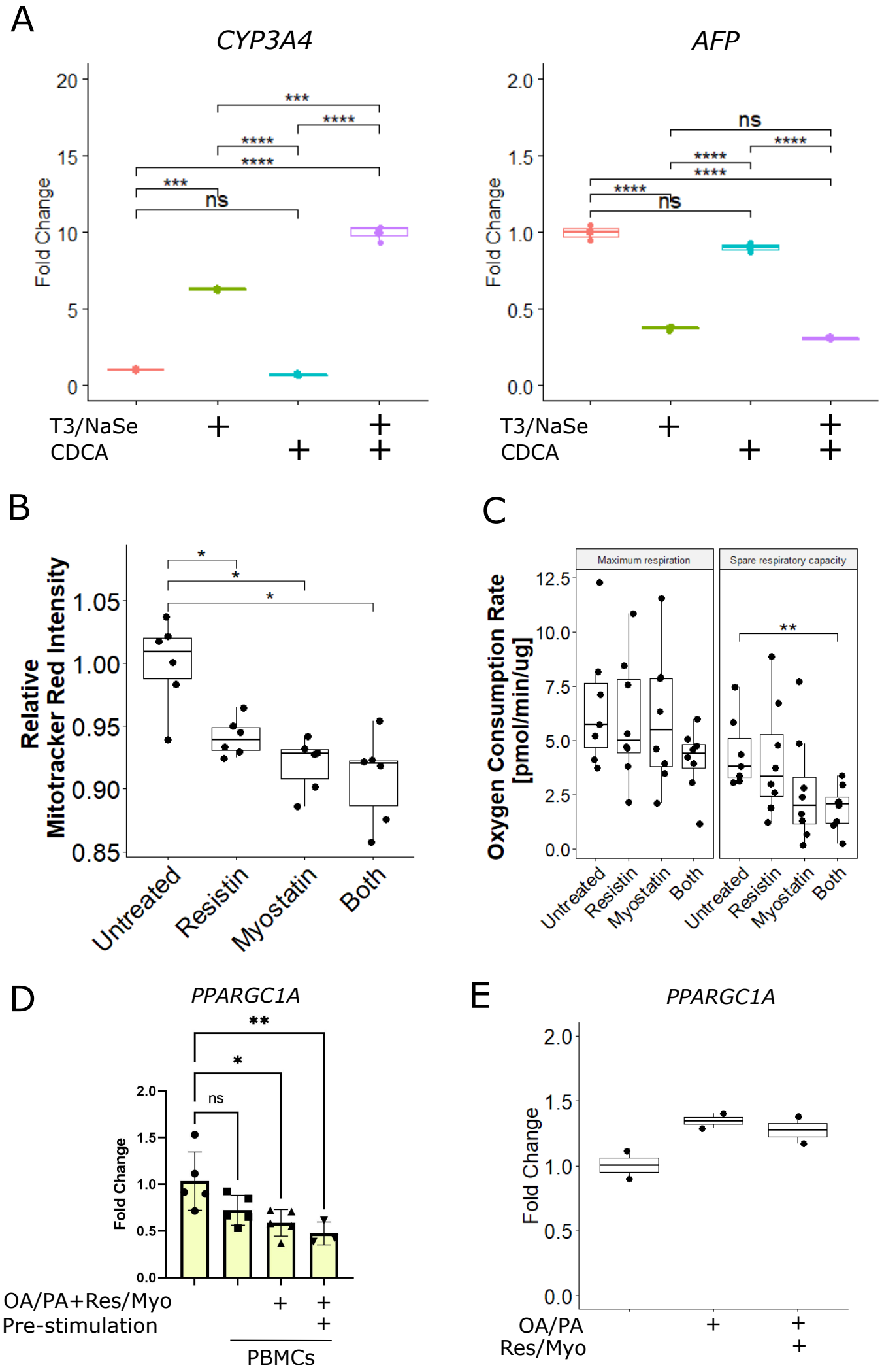
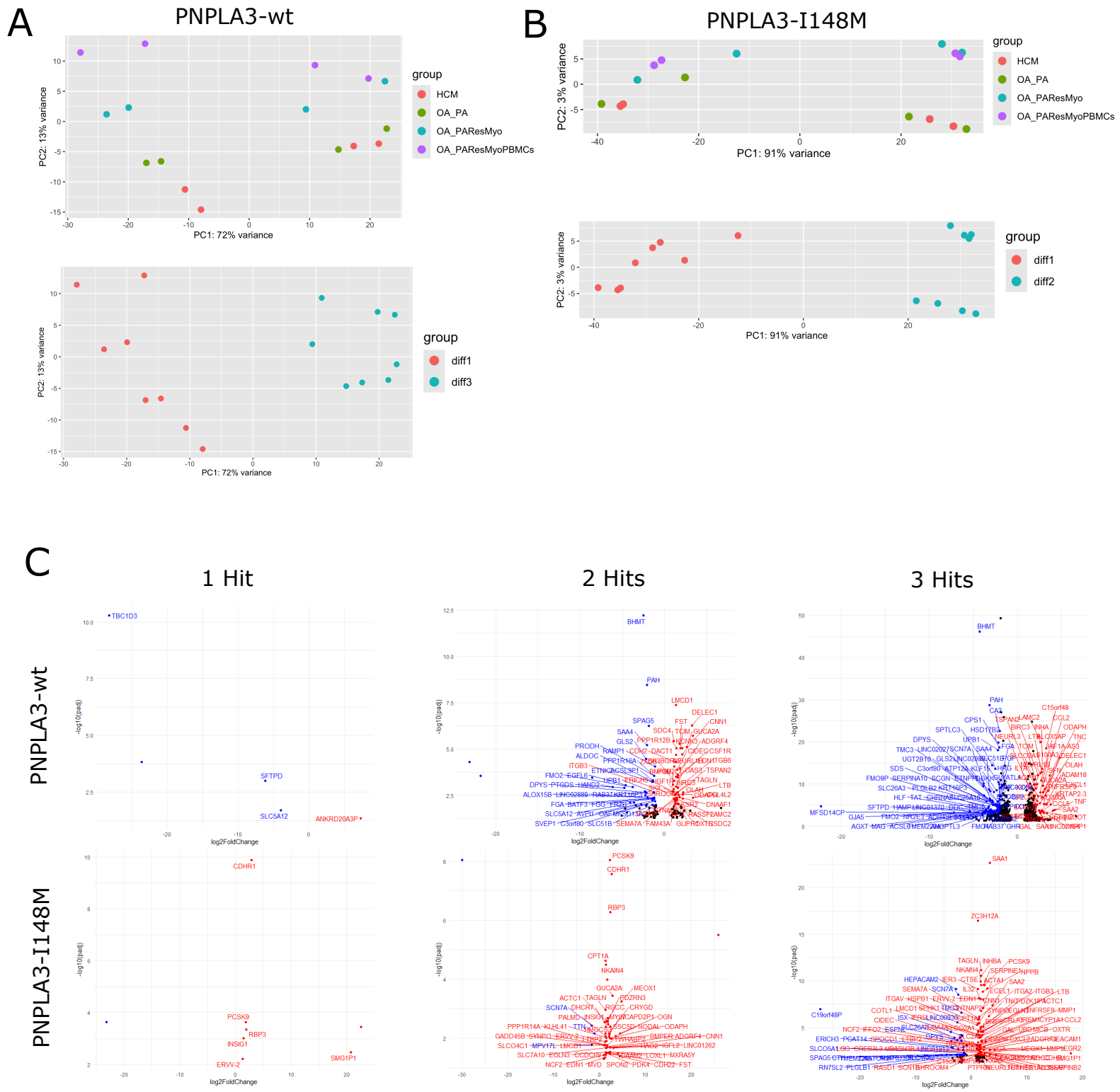
Supp. Figure 2: Transcriptomic changes in HLCs exposed to cumulative injury